**Atmospheric
Chemistry
and Physics
Discussions**

Optical and physical properties of aerosols in the boundary layer and free troposphere over the Amazon Basin during the biomass burning season

D. Chand[1], P. Guyon[1], P. Artaxo[2], O. Schmid[1], G. P. Frank[1], L. V. Rizzo[2], O. L. Mayol-Bracero[3], L. V. Gatti[4], and M. O. Andreae[1]

[1]Max Planck Institute for Chemistry, Mainz, Germany
[2]Institute of Physics, University of São Paulo, São Paulo, Brazil
[3]University of Puerto Rico, USA
[4]Institute of Nuclear Energy Research, São Paulo, Brazil

Correspondence to: D. Chand (duli@mpch-mainz.mpg.de)

4373

Abstract

As part of the Large Scale Biosphere-Atmosphere Experiment in Amazonia – Smoke, Aerosols, Clouds, Rainfall and Climate (LBA-SMOCC) campaign, detailed surface and airborne aerosol measurements were performed over the Amazon Basin during the dry to wet season from 16 September to 14 November 2002. Optical and physical properties of aerosols at the surface, boundary layer (BL) and free troposphere (FT) during the dry season are discussed in this article. Carbon monoxide (CO) is used as a tracer for biomass burning emissions. At the surface, good correlation among the light scattering coefficient (σ_s at 550 nm), PM2.5, and CO indicates that biomass burning is the main source of aerosols. Accumulation of haze during some of the large-scale biomass burning events led to high mass loadings (PM2.5=200 μg m^{-3}), σ_s (1400 Mm^{-1}), aerosol optical depth at 500 nm (3.0), and CO (3000 ppb). A few rainy episodes reduced the aerosol mass loading, number concentration (CN) and CO concentration by two orders of magnitude. The correlation analysis between σ_s and aerosol optical thickness shows that most of the optically active aerosols are confined to a layer with a scale height of 1660 m during the burning season. The average mass scattering and absorption efficiencies (532 nm) for small particles (diameter D_p< 1.5 μm) at surface level are found to be 5.3 and 0.42 m^2 g^{-1}, respectively, when relating the aerosol optical properties to PM2.5 aerosols. The observed mean single scattering albedo (ω_o at ~540 nm) for submicron aerosols at the surface (0.92±0.02) is significantly higher than reported previously. The scattering efficiency (dσ_s/dCN) of particles increases 2–10 times from the surface to the FT, most probably due to the combined affects of coagulation and condensation.

1 Introduction

The gas and particle emissions from tropical biomass burning influence the physical, chemical and optical properties of the atmosphere (Andreae et al., 1988; Crutzen and

4374

Andreae, 1990; Andreae and Crutzen, 1997; Hobbs et al., 1997; Artaxo et al., 1998; Andreae and Merlet, 2001; Ramanathan et al., 2001; Artaxo et al., 2001, 2002; Hobbs et al., 2003). Smoke aerosols contain a significant amount of partially oxidized organic material and black carbon or soot, which may have significant climatic implications

5 (IPCC, 2001). Aerosol particles interact directly with the incoming solar radiation by the scattering and absorption of light (Charlson et al., 1992; Rosenfeld, 2000; Andreae et al., 2004) and because they act as cloud condensation nuclei (CCN), thereby affecting indirectly the Earth's radiation budget. The importance of aerosol particles for climate forcing is recognized, but the magnitude of their contribution is highly uncertain (IPCC,

10 2001). It is thought that particles, through their combined direct and indirect effects, may currently have an influence of potentially similar magnitude, but opposite sign, as greenhouse gas forcing (IPCC, 2001). Aerosol radiative forcing may range from net heating to net cooling, depending on the aerosol properties as well as on the albedo of the underlying surface layer. Particles, with their short atmospheric lifetimes, have

15 significant vertical, horizontal and temporal gradients in their concentrations. These spatial gradients correspond to significant local/regional as well as global aerosol forcing effects. For example, smoke layers over the Amazon basin can have significant regional effects by reduction of regional photosynthetically active radiation up to 45% (Eck et al., 1998). Because of their light absorbing properties, the presence of aerosol

20 particles can result in the radiative forcing at the surface being much larger than at the top of the atmosphere (Satheesh and Ramanathan, 2000; Ramanathan et al., 2001; Procópio et al., 2003, 2004).

Biomass burning, particularly in the tropics, is a major source of atmospheric trace gases and particles (Andreae and Merlet, 2001). Being the world's largest rain forest

25 area containing approximately one quarter of all tropical rainforests, the Amazon Basin is subject to one of the highest rates of deforestation in the world (Artaxo, 2001; Gash et al., 1996). About 80% of the global burning activity is taking place in the tropics and one third of it occurs in South America alone. Under suitable meteorological conditions, the local chemical, physical, and optical characteristics of aerosols can be much different

4375

from the global or regional averages and these characteristics, in turn, are strongly influenced by local and regional sources and perturbations, e.g., forest emissions, fires, dust, sea salt, etc., leading to further spatial and temporal inhomogeneity.

Aerosol optical properties over the Amazon Basin have been studied in the previous

5 LBA and SCAR-B experiments (e.g., Eck et al., 1998, 2003; Kotchenruther and Hobbs, 1998; Martins et al., 1998; Reid et al., 1998; Reid and Hobbs, 1998; Ross et al., 1998; Guyon et al., 2003a; Guyon et al., 2004; Reid et al., 2004a, b). In these studies, the variability in the optical properties has been analyzed based on either surface or airborne measurements. However, so far, it is not understood how aerosol properties at

10 the surface relate to those aloft in the boundary layer and free troposphere. In addition to the limited surface observations, only a few series of in-situ vertical profile measurements of aerosol optical properties (e.g., light absorption, light scattering, hemispheric back-scattering) have been made over the Amazon Basin (e.g., Kotchenruther and Hobbs, 1998; Reid et al., 1998; Ross et al., 1998; Guyon et al., 2003a, 2003c; Reid

15 et al., 2004a, b). To our knowledge, almost no simultaneous observations of optical properties of aerosols and trace gases at the surface and aloft are available over the Amazon Basin in the biomass burning season.

This paper describes the vertical distribution of aerosol optical and physical properties over the Amazon Basin during the 2002 biomass burning season. The obser-

20 vations of light scattering (σ_s), light absorption (σ_a), aerosol optical thickness (AOT), aerosol number density (CN), aerosol mass concentration (PM2.5), and carbon monoxide (CO) are being used to address the following scientific questions: (1) How does σ_s vary at the surface, in the boundary layer and free troposphere? (2) How does σ_s vary vertically at different sites over the Amazon Basin? (3) How do Ångström expo-

25 nent observations from the airborne measurements compare with vertically integrated measurements using a sunphotometer?

4376

2   Instrumentation and methods

2.1   Observational sites

The measurements were made over the Amazon Basin during the Large Scale Biosphere-Atmosphere Experiment in Amazonia – Smoke, Aerosols, Clouds, Rainfall and Climate (LBA-SMOCC) from 16 September to 14 November in 2002. Detailed surface observations of aerosols and trace gases were made in the state of Rondônia, Brazil at a pasture site "Fazenda Nossa Senhora Aparecida" (10.76° S, 62.32° W, 315 m above mean see level (amsl)), hereafter FNS. This experimental site is located about 57 km north-west of the town of Ji-Paraná (10.88° S, 61.85° W, 235 m amsl). A few small hills (300–400 m height) are located about 1–4 km from FNS. One hill, known as "Abracos Hill", is one of the AERONET (Aerosol Robotic Network) sites and provides column integrated aerosol optical thickness (AOT) measurements using sun-photometry observations (Holben et al., 1998). Further details on the FNS site can be found elsewhere (Kirkman et al., 2002; Trebs et al., 2004). Airborne measurements in the boundary layer (BL) and free troposphere (FT, up to 4200 m) over the Amazon Basin were taken as far as 800 km from FNS. Some selected flight tracks along with the geographical location of the surface measurement site FNS are shown in Fig. 1. More details on this campaign are given in Andreae et al. (2004).

2.2   Measurements and methods

The surface observations at FNS over the Amazon basin were conducted from the middle of the smoky dry season (16 September) to the onset of the wet season (14 November), when pollution levels approached background conditions. In this study, we make use of ground based observations from 16 September to 8 October representing the biomass burning season during the SMOCC campaign.

Aerosol mass (PM2.5) and σ_s measurements at FNS were made using dry air (RH<40%) sampled from an inlet installed at about 10 m above the ground level. The

4377

σ_s and σ_a of dry aerosols at FNS were measured for the submicron size particles. An impactor with a cut off diameter at 1.5 μm was used to remove the bigger particles. Before selection through the impactor, the aerosols were dried by passing them through a Permapure Nafion drier. The drier unit and impactor (with and without impaction plate) were characterized for possible aerosol losses at the flow used. Most of the losses are confined to very small sizes that have very little effect on the measured σ_s and σ_a. Mie theory was used to calculate the effect of the losses. The loss of particles in terms of total σ_s and σ_a is 2–4% during the burning season. All the σ_s and σ_a data sets at FNS were corrected for these losses. The radiance research (RR) nephelometer, photoacoustic spectrometer (PAS) and particle soot absorption photometer (PSAP) were operating downstream of the impactor-drier units, and the losses observed by these instruments were of the same order.

Airborne measurements of aerosols and trace gases were made from 25 September to 19 October (about 31 flights). For this study, we make use of the airborne measurements of σ_s, aerosol number density (CN), size distribution (diameter, D_p=42–346 nm) and carbon monoxide (CO) from selected flights (numbers 4, 6, 7, 8 and 24), which include measurements conducted directly above FNS and its surroundings. The flight tracks of these observations along with dates are shown in Fig. 1 with complementary data in Table 2. Most of the flights were conducted during afternoon hours (14:00 LT=18:00 UT) when the depth of the BL was at its maximum level. Flights 6 and 7 were conducted on the same day during morning and afternoon hours, respectively. The measurements were taken up to a height of 4200 m. The time schedule of the studied parameters, their symbols, and further details on the surface and airborne observations are given in Tables 1–3. Some other details on the aircraft measurements can be found in Guyon et al. (2005).

The time resolution of the σ_s and σ_a measurements at FNS was one minute; they were processed to get higher averaging intervals (30 min) to match the averaging time of the aerosol mass (PM2.5) measurement. A real-time aerosol mass monitor, the Tapered Element Oscillating Microbalance (TEOM, series 1400a, Rupprecht & Patash-

4378

nick Inc.) was used to measure PM2.5 aerosol mass concentration with a time resolution of 30 min. The TEOM inlet was heated to 50°C for drying the aerosols. The aerosol number density was measured using a TSI condensation particle/nuclei (CN) counter (model 3022A) with a minimum detection size of 8 nm. CO was measured with the Thermo Environmental Instrument Inc. analyzer (Model 48C Gas Filter Correlation) with a minimum detection limit of 40 ppb. Because of the high ambient humidity, a cooler was used to remove water from the sample stream prior to the CO analyzer. The CO measurements on the aircraft were made using an Aero-Laser (AL5002) instrument operating at 1 Hz. Prior to sampling, the air was dried using a Nafion drier.

Under suitable wind conditions, the transport of pollutants from fossil fuel combustion (like cars and trucks from a nearby road) contaminated the data for short periods. The time periods with winds coming from the direction of the road, having high CO, nitric oxides (NO_x) and low single scattering albedo (ω_o) were assumed to be affected by cars and trucks; these data (<5% of the total data set) were removed and not considered in this study. 30-min average aerosol properties, for instance, σ_s, σ_a, AOT and PM2.5 were used to derive the intensive optical properties like ω_0, mass scattering efficiency (α_s), mass absorption efficiency (α_a) and Ångström exponent ($\overset{0}{a}$). The dry size distribution of aerosols (10–414 nm) in the BL and FT was measured using a TSI scanning mobility particle sizer (SMPS model 3936). The size scans were made over 2 min each. The next section describes the details of the methods and measurements used to derive the optical properties.

2.3 Aerosol optical properties

2.3.1 Aerosol light scattering

The light scattering properties of the dry aerosols were measured using Radiance Research (RR, model M903) and TSI (TSI, model 3563) nephelometers. The RR nephelometer measures σ_s at a single wavelength (545 nm) whereas the TSI nephelometer measures σ_s at three wavelengths (450, 550, 700 nm). The RR nephelometers were

employed for observations on the ground at FNS. The TSI nephelometer was used for airborne observations. The calibrations of the nephelometers and the basic measurement strategy adopted herein have been described by Anderson and Ogren (1998). The nephelometers were calibrated during the field campaign using particle-free air and CO_2 as a span gas. All the nephelometers were inter-compared by running them parallel to each other after the end of the airborne campaign; agreement was found to be within 5%. Measurements of the total scattering coefficient in the RR and TSI nephelometers cover the angles 9–170° and 7–170°, respectively. The RR nephelometer data at FNS are corrected for the truncated angles using Mie calculations. The truncated angles (0–9°, 170–180°) contribute about 4% of the total light scattering by the dry fine aerosols ($D_p<1.5\,\mu$m) in the biomass burning season. However, σ_s is not corrected for truncation errors for the airborne observations using the TSI nephelometer. The truncation angles in the TSI nephelometer are smaller (0–7°, 170–180°) compared to the RR nephelometer. Based on the Mie calculations we performed and also on Guyon et al. (2003c), the contribution by the truncated angles may be 4–16% of the total light scattering by ambient aerosols. All the data from both the nephelometers (RR and TSI) presented in this article are converted to a standard temperature (25°C) and pressure (1000 hPa) using the method described by Anderson and Ogren (1998). The estimated combined accuracy of σ_s is <10%.

The spectral dependence of σ_s can be derived from the multi-wavelength (TSI nephelometer) measurements. This dependence is an intensive parameter in the sense that it depends on the aerosol size distribution and refractive index but, contrary to σ_s(at a wavelength λ) not on the aerosol concentration. It is generally assumed that the wavelength dependence of the scattering coefficient from the nephelometer can be described in the visible spectrum by an empirical equation as a power law of λ (Ångström, 1929):

$$\sigma_s(\lambda) = \beta_s \lambda^{-\overset{0}{a}_s}, \tag{1}$$

where $\sigma_s(\lambda)$ is the scattering coefficient at wavelength λ, β_s is a constant, and $\overset{0}{a}_s$ is

the non-dimensional Ångström exponent. In order to cover the widest possible spectral range, we compute $\overset{0}{a}_s$ from the nephelometer measurements at 450 nm and 700 nm to obtain $\overset{0}{a}_s$ i.e.,

$$\overset{0}{a}_s = -\frac{\log(\sigma_s(\lambda_1)/\sigma_s(\lambda_2))}{\log(\lambda_1/\lambda_2)} \; . \tag{2}$$

The variability in $\overset{0}{a}_s$ can be used to provide an insight on the types of aerosol from the nephelometer observations, since Mie theory shows that $\overset{0}{a}_s$ increases with decreasing aerosol particles size. For instance, $\overset{0}{a}_s$ values for fine anthropogenic aerosol encountered in polluted areas are typically larger than 1, whereas $\overset{0}{a}_s$ is close to zero in regions dominated by coarse mode desert dust (Horvath and Trier, 1993; Eck et al., 1999). The mass scattering efficiency α_s is derived by normalizing the scattering coefficient σ_s with PM2.5 obtained from the TEOM.

2.3.2 Aerosol light absorption

The σ_a of aerosol particles was measured by a Particle Soot Absorption Photometer (PSAP) calibrated using a Photoacoustic spectrometer (PAS) as a reference. The PSAP measures σ_a based on the attenuation of light (565 nm) through a particle-loaded filter. Although Bond et al. (1999) have provided a calibration for the PSAP using laboratory-generated model aerosols, its validity for atmospheric aerosol is questionable, since the calibration is likely to depend on parameters such as aerosol size, single scattering albedo and RH (Arnott et al., 2003). In order to correct the systematic error encountered with the PSAP, we calibrated the PSAP in the field with a PAS (Arnott et al., 1999), which measures σ_a (532 nm) on the airborne aerosol by converting the absorbed energy into an acoustic wave (Terhune and Anderson, 1977). For PSAP calibration, the PAS and PSAP were operated in parallel for several days during

4381

the campaign. In contrast to filter-based methods like the PSAP, the PAS measurement is performed on particles in their suspended state, i.e., sampling artifacts due to filter-particle interactions are avoided. To avoid potential complications in both PAS and PSAP due to elevated RH (Arnott et al., 2003), both the instruments were operated with dry aerosol (RH <50%). The known PAS cross-sensitivity to NO_2 (Arnott et al. 2000) was corrected based on continuous NO_2 measurements with a NO_x analyzer (Trebs et al., 2005). Laboratory studies with soot and biomass burning aerosols have shown good agreement between the PAS and an optical extinction cell (Schnaiter et al., 2004). We estimated the combined accuracy of σ_a measurements to be <10%. Further details on the σ_a measurements can be found in Chand et al. (2005)[1].

Analogous to α_s, the mass absorption efficiency (α_a) is computed by normalizing σ_a with the aerosol mass concentration obtained from PM2.5. Furthermore, the single scattering albedo (ω_0) is defined as

$$\omega_0 = \frac{\sigma_s}{\sigma_s + \sigma_a} \; . \tag{3}$$

As pointed out earlier, the light scattering and absorption coefficients (i.e. σ_s, σ_a) measured at 545 nm and 532 nm, respectively, giving ω_0 at 540 nm.

2.3.3 Aerosol optical thickness

A sunphotometer (CIMEL, model CE 318-1) described by Holben et al. (1998) was set up on Abracos hill about 4 km from the ground station FNS as a part of the AERONET network. The sunphotometer is used to measure column aerosol optical thickness (AOT) at 7 wavelengths (340, 380, 440, 500, 670, 870 and 1020 nm). The AOT data have been screened for cloud events according to a standardized procedure (Smirnov et al., 2000). The value of the AOT is indicative of the extinction of the solar radiation

---

[1]Chand, D., Schmid, O., Vestin, A., Artaxo, P., Frank, G. P., Guyon, P., Gatti, L. V., Swietlicki, E., and Andreae, M. O.: Diurnal and seasonal variations in optical and physical properties of aerosols at a pasture site over the Amazon Basin, in preparation, 2005.

4382

due to the columnar aerosol content and, similar to σ_s, the wavelength dependence of AOT can be expressed by a power law empirical equation (Ångström, 1929):

$$AOT(\lambda) = \beta_e \lambda^{-\overset{0}{a_e}},\tag{4}$$

where

$$\overset{0}{a_e} = -\frac{\log AOT(\lambda_1)/AOT(\lambda_2)}{\log(\lambda_1/\lambda_2)}\tag{5}$$

To calculate the Ångström exponent ($\overset{0}{a_e}$), we will be using the AOT at two wavelengths, 440 nm and 670 nm, which are very close to the $\overset{0}{a_s}$ wavelengths (450, 700 nm) measured by the nephelometer. The Ångström exponents from two independent methods ($\overset{0}{a_s}$, $\overset{0}{a_e}$) provide information on the aerosol size distribution averaged over height during the airborne observations as well as over the column of the atmosphere using the AOT measurements.

2.3.4 Excess ratios

The method for calculation of excess ratio (ER) is discussed in detail in Andreae and Merlet (2001) and in Le Canut et al. (1996), i.e., where *dy/dx* is the slope of correlation of species "*y*" with respect to "*x*" in a biomass burning environment (plume and/or haze mixed in the background air). The advantage of this method is that it is not necessary to estimate the background concentration of the species while computing the ER. Equation 6 is used to calculate the excess ratios of σ_s to CO, σ_s to CN, σ_s to PM2.5, and σ_a to PM2.5 for both the regional haze as well as smoke plumes.

3 Results and discussions

3.1 Measurements at the ground site FNS

Figure 2 shows the 30-min averaged time series of σ_s, σ_a, PM2.5 and CO for the burning season at FNS. A large variability of 2 orders of magnitude is observed in σ_s, σ_a, PM2.5, and CO with values ranging 5–1400 Mm^{-1}, 1–70 Mm^{-1}, 2–200 μg m^{-3} and 300–3500 ppb, respectively. The highest levels in σ_s, σ_a, PM2.5 and CO were observed during the heavily burning-influenced periods on 21, 25–26 September and 5 October (see Fig. 2). The lower values were typically observed after the rain events (e.g., 20 September, 28 September–2 October). Some of the rainfall events, for instance on 28 September (vertical bars, Fig. 2), resulted in dramatic reduction of aerosol and CO concentrations. The simultaneous decrease in concentrations of aerosols and CO indicates that the clean-up was due to air mass replacement followed by fire suppression, while the role of scavenging was likely low. Since most of the period (16 September– 8 October) is dominated by biomass burning aerosols (except for a few rain events), the aerosol properties along with CO are representative of biomass burning conditions.

Figure 3 shows the correlations of σ_s with PM2.5, CN, CO and also σ_a with PM2.5 at the pasture site FNS during the burning period. The σ_s and σ_a of the aerosols are positively correlated with PM2.5, CN and CO. Good correlation is found between σ_s and PM2.5 (r^2=0.93) as well as between σ_s and CO (r^2=0.87). The correlation between σ_a and PM2.5 (r^2=0.70) is not as good as for σ_s and PM2.5. Poor correlation (r^2=0.30) is observed between σ_s and CN.

The slopes of σ_s and σ_a with PM2.5 (dσ_s/dPM2.5, dσ_a/dPM2.5) are the average mass scattering efficiency (α_s) and mass absorption efficiency (α_a), 5.3 and 0.42 m^2 g^{-1}, respectively, during the burning period. We note here that since the cut point (D_p) for the measurements of σ_s and σ_a is 1.5 μm, compared to PM2.5, our values are a lower estimate of the true α_s and α_a for these particles. The mass between PM1.5 and PM2.5 is less than 10% of PM2.5 during the dry season (Chand et al., 2005[1]).

The average ω_o, calculated using Eq. (3), is about 0.92±0.02. This value is significantly higher than the observations in earlier campaigns. Also, the ω_o and other optical parameters showed pronounced diel variations, which will be discussed in detail in Chand et al. (2005)[4]. The hourly average values of ω_o at midnight (00:00 local time, LT) and midday (12:00 LT) are 0.91±0.02 and 0.94±0.02, respectively. The daytime aerosols are representative of a deep mixing layer height (~1600 m) with longer transport times than night time aerosols with a mixing layer height of about 200 m. Due to different mixing and transport times in the BL during day and night, the daytime aerosols are generally more aged than the aerosols in night time. Observations of higher scattering efficiency for the aerosols at higher altitudes compared to those near ground (Sect. 3.2) corroborate our observation of higher ω_o during day time.

Using CO as a conservative tracer of biomass burning (Andreae and Merlet, 2001), the good correlation between σ_s and CO indicates that most of the aerosols which contribute to σ_s have originated from biomass combustion. Also, good correlations of σ_s with PM2.5 and CO indicate that the scattering efficiency from the haze particles is relatively independent of the absolute pollution level during the burning period. Even though the correlation between σ_s and CN is not good at FNS, the slope ($d\sigma_s/dCN=0.03\,Mm^{-1}$ per particle per cm^3) gives some insight into the amount of light scattered per CN. The poor correlation coefficient between σ_s and CN is due to the large variability in the very small particles (<40 nm), which make a negligible contribution to light scattering (Chand et al., in preparation, 2005[4]).

The average mass scattering efficiency ($\alpha_s=5.3\,m^2\,g^{-1}$) of the submicron dry aerosols observed in this study is consistent with the earlier observations during the LBA-EUSTACH 2 campaign in September-October, 1999 over the Amazon Basin (Guyon et al., 2003b). However, the mass absorption efficiency ($\alpha_a=0.42$) in this study is about 35% higher than during the LBA-EUSTACH 2 campaign. The airborne observations of relatively young aerosols during the "Smoke Clouds Aerosols and Radiation Brazil" (SCAR-B) campaign showed a much lower α_s (2.8–3.6 $m^2 g^{-1}$) and higher α_a (0.7–1.1) over the Amazon Basin (Reid et al., 1998a, 1998b). These levels of α_s ob-

4385

served from young aerosols (few minutes to less than an hour) during the SCAR-B experiment are much lower than our observations representing relatively more aged aerosols (regional haze). The differences in observations of α_a in this study with the LBA-EUSTACH 2 and SCAR-B observations may be due to different burning conditions (flaming vs. smoldering) and different aging processes. The other possibility for the difference with LBA-EUSTACH 2 and SCAR-B measurements is the much better instrumentation available nowadays than in 1995, in particular for σ_a measurements using PAS, as discussed in Sect. 2.3.2.

3.2 Airborne Measurements

The vertical structure and evolution in the σ_s of the aerosols from biomass burning can be assessed by measuring it along with other parameters (e.g., CN, CO) at the surface and aloft in the BL and FT. For example, correlations of σ_s with CO at different altitudes can be used to get some insights on mixing/dilution of the aerosols when the air is transported from the BL to the FT. Similarly, correlations of σ_s with CN at different altitudes can be used to get some information on evolution/ageing (coagulation, condensation, etc.) of the aerosols when the air is transported from the BL to the FT.

Figures 4a, c and e show scatter plots of σ_s against CN from the airborne observations for flights 4, 6, 7, 8 and 24, covering a large area over the Amazon Basin (see the flight tracks in Fig. 1). The slopes ($d\sigma_s/dCN$) in the BL and FT represent the scattering efficiency of aerosols for the respective flights. Depending on the altitude and nature of the aerosols (haze or fresh plumes), the slopes ($d\sigma_s/dCN$) may vary significantly (see Table 2).

Similar to the variations at ground level at FNS, σ_s is positively correlated with CN in the BL as well as in the FT. However, unlike at FNS, the airborne observations show a better correlation coefficient (higher r^2) between σ_s and CN and show two modes/slopes during most of the flights. These two modes, as shown by the slopes in Figs. 4a, b, c, e, and f, could be related to two types of aerosols in the BL and FT. The good correlation (high r^2) in both modes indicates that, in contrast to our findings

4386

at the surface site, most of the particles become optically active and contribute to light scattering when transported up to the BL and FT.

The transition between the two modes takes place between 1200 and 2000 m, at a mean height of 1600 m amsl. The aerosol below 1600 m amsl shows a lower $d\sigma_s$/dCN, whereas it is much higher above this height during all these flights. The scattering per particle at 550 nm in the FT is 1.6 to 11 times higher than in the BL (see Table 2). Depending on the size of the aerosols in the BL and FT, $d\sigma_s$/dCN may further increase by up to 16% when the scattering from the truncated angles is included. The transition altitude between the two modes is close to the BL height at the pasture site over the Amazon Basin (Guyon et al., submitted, 2005[1]). Earlier observations of the BL height over this site in the burning season are ~1650 m (above ground) as discussed by Fisch et al. (2004).

Figures 4b, d and f show the correlation of σ_s with CO from the airborne observations for flights 4, 6, 7, 8 and 24. A summary of the $d\sigma_s$/dCO at 550 nm in the BL and FT is also given in Table 2. Similar to the observations at the ground (FNS), the light scattering is positively correlated with CO in the BL with a slope ($d\sigma_s$/dCO) in the range of 0.36–0.40 Mm^{-1} ppb^{-1}. It is interesting to note here that the variability in the range of $d\sigma_s$/dCO is much lower than in $d\sigma_s$/dCN. The clear difference in slope between BL and FT observed in $d\sigma_s$/dCN in all of the flights (Fig. 4) is evident for $d\sigma_s$/dCO only during flights 4 and 24. The ratio of correlation slopes $(d\sigma_s/dCO)_{FT}/(d\sigma_s/dCO)_{BL}$ in the BL to the FT varies between 2.8 and 3.8 at 550 nm, probably as a result of variations in aerosol processing (coagulation and hygroscopic growth). The slopes ($d\sigma_s$/dCO) are very similar in the BL for all flights with a mean value of 0.38 Mm^{-1} ppb^{-1}. This value from the airborne observations is very close to the surface observations at FNS ($d\sigma_s$/dCO=0.42 Mm^{-1} ppb^{-1}). Slightly lower levels of airborne $d\sigma_s$/dCO in the BL may be due to the underestimation of σ_s by not considering the light scattering from truncated angles. A good agreement in $d\sigma_s$/dCO between the ground and airborne observations in the BL covering a large area suggests that the biomass burning aerosol sampled at FNS reflects sources typical for the entire region, with similar emission

4387

characteristics as over the rest of the Amazon Basin (Table 2).

Comparing the variations of σ_s with CN and CO in the BL and FT, the vertical change is larger in $d\sigma_s$/dCN than in $d\sigma_s$/dCO (Table 2). The increase of $d\sigma_s$/dCO from the BL to the FT may be attributable to particle growth during aging. The fact that $d\sigma_s$/dCN increases even more suggests a substantial reduction in the relative abundance of small, weakly scattering particles in the FT relative to the BL.

The observations regarding $d\sigma_s$/dCO and $d\sigma_s$/dCN are at least in part reflected in an analysis of the trends in particle volume as a function of altitude. Figure 5 shows the total number normalized volume (D_p=42–346 nm) of dry aerosols as a function of height during flights 4, 6, 7, 8 and 24. The volume per unit ambient aerosol ($V_n=V_{total}/N_{total}$) increases with height with a peak at 2000–3000 m (700-800 hPa) during all the flights. The ratios of maximum V_n in FT (~2500 m) to the lowest V_n in BL (500 m) varies from 1.3–1.6 (factor "C" in Table 2). The overall trends in V_n for flights 6, 7, 8 are consistent with those for flights 4 and 24, but V_n is higher in flights 4 and 24 compared to flights 6, 7 and 8. The higher V_n is consistent with higher $d\sigma_s$/dCN during the flights 4 and 24. The relatively low RH (<60%) for most of the flights suggests that the contribution of humid growth in increasing V_n and σ_s is minor (Guyon et al., submitted, 2005[1]). Higher aerosol volume aloft suggests that condensation of organic and possibly inorganic vapors, as well as coagulation, plays an important role in changing the physical (size) properties (Table 2).

Some meteorological conditions (e.g., a strong BL inversion as observed on Flight 4 and 24), can increase the difference in $d\sigma_s$/dCN between the BL and FT. The strong inversion reduces the transport/mixing of air from the FT to the BL, and the ageing of the aerosols in the FT increases V_n and $d\sigma_s$/dCN. Assuming that σ_a per particle is independent of altitude, the increased $d\sigma_s$/dCN corresponds to an increase in ω_o up to 7% (from 0.92 to 0.98) for the aerosols in the FT. This assumption is corroborated by the lower ω_o during the night hours (0.91) and the higher ω_o in day time (0.94). More details of the diurnal variation in optical properties of aerosols at the surface site (FNS) over the Amazon Basin is being included in another manuscript under prepara-

4388

tion (Chand et al., 2005[4]).

3.3 Vertically integrated measurements

In order to determine whether the characteristics of aerosols measured by sunphotometry at the ground agree with in-situ measurements in the atmospheric column (BL and FT), we compared the Ångström exponents derived from independent sunphotometer and aircraft measurements (i.e., a_e^0 and a_s^0) (Table 3). The mean airborne a_s^0 from the individual flights vary in the range of 1.9 to 2.1 whereas the column integrated a_e^0 varies in the range of 1.4 to 2.0. The mean values of a_e^0 and a_s^0 are 2.0±0.4 and 1.8±0.1, respectively. The small difference between a_e^0 and a_s^0 suggests that the sunphotometer results at FNS are regionally representative, and that the aerosols in the FT above the ceiling height of the aircraft did not significantly influence the value of a_e^0.

Convective activity enhances the vertical mixing and transport of aerosols in the atmosphere during the dry/burning period. An indication of the vertical extent of the aerosol column during the burning dominated period can be provided by an aerosol index called "optical scale height" (OSH). OSH is defined as the height (in m) of a homogeneous aerosol column having the same extinction coefficient ($\sigma_{ext} = \sigma_s + \sigma_a$) as the one determined at ground level, and the same AOT as the one measured by the sunphotometer. A plot of AOT (550 nm) vs. σ_s at FNS (AOT is adjusted to the same wavelength as σ_s using Eqs. (4) and (5) yields a slope corresponding to an OSH of 1660. This indicates that most of the optically active aerosols are confined to lower heights (i.e., the BL) during the burning period.

4 Summary and Conclusions

Detailed ground and airborne measurements were taken over the Amazon Basin during the LBA-SMOCC experiment conducted during the dry season (September–October 2002). These results have shed new light on the optical and physical properties of biomass burning aerosols. The relationships between observations at the ground and in the BL and FT have been investigated.

In general, all the aerosol extensive properties and CO showed large variability during the biomass burning season. During some of the most intensive burning periods, very high mass loading (PM2.5 >200 μg m^{-3}) resulted in scattering coefficients as high as 1400 Mm^{-1} at 550 nm. At the same time, the aerosol optical depth at 500 nm reached values of more than 3 and CO exceeded 3000 ppb. A few rain events reduced the aerosol loadings and optical effects by two orders of magnitude.

The mass scattering and absorption efficiencies, α_s and α_a, relative to PM2.5 aerosols at about 550 nm at the ground are found to be 5.3 and 0.42 m^2 g^{-1}, respectively. The observed ω_o at 540 nm is 0.92±0.02. The dσ_s/dCN in the free troposphere (between 1600 to 4200 m amsl) is about 1.6 to 10.9 times higher than in the BL (below 1600 m amsl). Assuming the same absorption efficiency of aerosols with altitude, this increase of σ_s in the FT can increase ω_o up to 7% from 0.92 to 0.98.

The Ångström exponent (2.0±0.4) computed from the airborne observations below 4200 m is insignificantly higher than the Ångström exponent (1.8±0.1) calculated by column integrated (sunphotometer) measurements. This suggests that aerosol properties measured at our ground site are regionally representative, and that the aerosol above 4200 m does not strongly affect the column-integrated Ångström exponent.

The strong correlation of σ_s with PM2.5 and CO indicates that Eq. (1) most of the aerosol mass has originated from biomass combustion and Eq. (2) the smoke-laden air with different CO and mass loading has similar source (same α_s) and emission characteristics. The σ_s does not correlate well with the aerosol number concentration (CN) at the ground, however, it has a better correlation aloft in the BL and FT. This

indicates that the ageing process plays an important role in the optical and physical properties of aerosols.

The correlation analysis between σ_a and aerosol AOT suggests that most of the aerosols are confined to the lower levels of the atmosphere (<1660 m) during the burning season. Similar levels of $d\sigma_s/dCO$ between surface and airborne observations covering a large area in the BL again suggest that the burning activities over the Amazon Basin have similar sources and fuel emission characteristics. Larger variation in σ_s with CN than with CO, as shown by the numbers A and B, respectively in Table 2, suggest that condensation-coagulation plays an important role in changing the radiative properties of aerosols. The scattering efficiency of aerosols (V_n) increases with height, having a maximum at 1700–3000 m.

This is the first study presenting a comprehensive data set on optical properties of aerosols at the ground, BL and FT in the dry season over the Amazon Basin. This data set, along with the data from the SCAR-B and LBA-EUSTACH2 campaigns covering a limited area, can be used to validate the optical parameters retrieved from satellites. The validated optical properties obtained from satellites can then be used to derive the optical parameters over the large area of the entire Amazon Basin. The combined ground, airborne and remote sensing observations can be valuable to assess the role of biomass burning and its impact at local, regional and global scales.

4391

References

Andreae, M. O., Browell, E. V., Garstang, M., Gregory, G. L., Harriss, R. C., Hill, G. F., Jacob, D. J., Pereira, M. C., Sachse, G. W., Setzer, A. W., Dias, P.L.S., Talbot, R. W., Torres, A. L., and Wofsy, S. C.: Biomass-burning emissions and associated haze layers over Amazonia, J. Geophys. Res.-Atmos., 93, 1509–1527, 1988.

Andreae, M. O. and Crutzen, P. J.: Atmospheric aerosols: Biogeochemical sources and role in atmospheric chemistry, Science, 276, 1052–1058, 1997.

Andreae, M. O. and Merlet, P.: Emission of trace gases and aerosols from biomass burning, Global Biogeochem. Cycles, 15, 955–966, 2001.

Andreae, M. O., Artaxo, P., Brandao, C., Carswell, F. E., Ciccioli, P., da Costa, A. L., Culf, A. D., Esteves, J. L., Gash, J. H. C., Grace, J., Kabat, P., Lelieveld, J., Malhi, Y., Manzi, A. O., Meixner, F. X., Nobre, A. D., Nobre, C., Ruivo, M., Silva-Dias, M. A., Stefani, P., Valentini, R., von Jouanne, J., and Waterloo, M. J.: Biogeochemical cycling of carbon, water, energy, trace gases, and aerosols in Amazonia: The LBA-EUSTACH experiments, J. Geophys. Res.-Atmos., 107, D20, 8066, doi:10.1029/2001JD000524, 2002.

Andreae, M. O., Rosenfeld, D., Artaxo, P., Costa, A. A., Frank, G. P., Longo, K. M., and Silva-Dias, M. A. F.: Smoking Rain Clouds over the Amazon, Science, 303, 1337–1342, 2004.

Anderson, T. L. and Ogren, J. A.: Determining aerosol radiative properties using the TSI 3563 integrating nephelometer, Aerosol Sci. Technol., 29, 57–69, 1998.

Ångström, A.: On the atmospheric transmission of Sun radiation and on dust in the air, Geogr. Ann., 12, 130–159, 1929.

Artaxo, P., Fernandes, E. T., Martins, J. V., Yamasoe, M. A., Hobbs, P. V., Maenhaut, W., Longo, K. M., and Castanho A.: Large Scale Aerosol Source Apportionment in Amazonia, J. of Geophys. Res., 103, D24, 31 837–31 848, 1998.

Artaxo, P.: The atmospheric component of biogeochemical cycles in the Amazon basin, in: The biogeochemistry of the Amazon basin, edited by: McClain, M. E., Victória, R., Richey, J. E., Oxford University Press, 42–52, 2001.

Artaxo, P., Martins, J. V., Yamasoe, M. A., Procópio, A. S., Pauliquevis, T. M., Andreae, M. O., Guyon, P., Gatti, L. V., and Leal, A. M. C.: Physical and chemical properties of aerosols in the wet and dry seasons in Rondônia, Amazonia, J. Geophys. Res.-Atmos., 107(D20), 8081, doi:10.1029/2001JD000666, 2002.

Arnott, W. P., Moosmüller, H., Rogers, C. F., Jin, T., and Bruch, R.: Photoacoustic spectrometer

4392

for measuring light absorption by aerosols: Instrument description, Atmos. Environ., 33, 2845–2852, 1999.

Arnott, W. P., Moosmüller, H., and Walker, J. W.: Nitrogen dioxide and kerosene-flame soot calibration of photoacoustic instruments for measurement of light absorption by aerosols, Review Scient. Instrum., 71, 4545–4552, 2000.

Arnott, W. P., Moosmüller, H., Sheridan, P. J., Ogren, J. A., Raspet, R., Slaton, W. V., Hand, J. L., Kreidenweis, S. M., and Collett Jr., J. L.: Photoacoustic and filter-based ambient aerosol light absorption measurements: Instrument comparisons and the role of relative humidity, J. Geophys. Res.-Atmos., 108(D1), 4034, doi:10.1029/2002JD002165, 2003.

Arnott, W. P., Khadeejeh, H., Moosmüller, H., Sheridan, P. J., and Ogren, J. A.: Towards aerosol light-absorption measurements with a 7-wavelength aethalometer: Evaluation with a photoacoustic instrument and 3-wavelength nephelometer, Aerosol Sci. Technol., 39, 17–29, 2005

Bond, T. C., Anderson, T. L., and Campbell, D.: Calibration and intercomparison of filter-based measurements of visible light absorption by aerosols, Aerosol Sci. Technol., 30(6), 582–600, 1999.

Charlson, R. J., Schwartz, S. E., Hales, J. M., Cess, R. D., Coakley, J. A., Hansen, J. E., and Hoffman, D. J.: Climate forcing by anthropogenic aerosols, Science, 255, 423–430, 1992.

Crutzen, P. J. and Andreae, M. O.: Biomass burning in the tropics: Impact on atmospheric chemistry and biogeochemical cycles, Science, 250, 1669–1678, 1990.

Eck, T. F., Holben, B. N., Slutsker, I., and Setzer, A.: Measurements of irradiance attenuation and estimation of aerosol single scattering albedo for biomass burning aerosols in Amazonia, J. Geophys. Res.-Atmos., 103, 31 865–31 878, 1998.

Eck, T. F., Holben, B. N., Reid, J. S., Dubovik, O., Smirnov, A., O'Neill, N. T., Slutsker, I., and Kinne, S.: The wavelength dependence of the optical depth of biomass burning, urban and desert dust aerosols, J. Geophys. Res, 104, 31 333–31 350, 1999.

Eck, T. F., Holben, B. N., Reid, J. S., O'Neill, N. T., Schafer, J. S., Dubovik, O., Smirnov, A., Yamasoe, M. A., and Artaxo, P.: High aerosol optical depth biomass burning events: A comparison of optical properties for different source regions, Gepohys. Res. Lett., 30, No. 20, 2035, doi:10.1029/2003GL017861, 2003.

Fisch, G., Tota, J., Machado, L. A. T., Silva Dias, M. A. F., da F. Lyra, R. F., Nobre, C. A., Dolman, A. J., and Gash, J. H. C.: The convective boundary layer over pasture and forest in Amazonia, Theor. Appl. Climatol., doi:10.1007/s00704-004-0043-x, 78, 47–59 2004.

Gash, J. H. C., Nobre, C. A., Roberts, J. M. and Victoria, R. L.: Amazonian deforestation and

4393

climate, John Wiley & Sons Ltd, Chichester, England, 1996.

Gras, J. L., Jensen, J. B., Okada, K., Ikegami, M., Zaizen, Y. and Makino, Y.: Some optical properties of smoke aerosol in Indonesia and tropical Australia, Geophys. Res. Lett., 26, 1393–1396, 1999.

Guyon, P., Boucher, O., Graham, B., Beck, J., Mayol-Bracero, O. L., Roberts, G. C., Maenhaut, W., Artaxo, P., and Andreae, M. O.: Refractive index of aerosol particles over the Amazon tropical forest during LBA-EUSTACH 1999, J. Aerosol Sci., 34(7), 883–907, 2003a.

Guyon, P., Graham, B., Roberts, G. C., Mayol-Bracero, O. L., Maenhaut, W., Artaxo, P., and Andreae, M. O.: In-canopy gradients, composition, sources, and optical properties of aerosol over the Amazon forest, J. Geophys. Res.-Atmos., 108(D18), 4591, doi:10.1029/2003JD003465, 2003b.

Guyon, P., Graham, B., Beck, J., Boucher, O., Gerasopoulos, E., Mayol-Bracero, O. L., Roberts, G. C., Artaxo, P., and Andreae, M. O.: Physical properties and concentration of aerosol particles over the Amazon tropical forest during background and biomass burning conditions, Atmos. Chem. Phys., 3, 951–967, 2003c, SRef-ID: 1680-7324/acp/2003-3-951.

Guyon, P., Graham, B., Roberts, G. C., Mayol-Bracero, O. L., Maenhaut, W., Artaxo, P., and Andreae, M. O.: Sources of optically active aerosol particles over the Amazon forest, Atmos. Environ., 38 1039–1051, 2004.

Guyon, P., Frank, P., Welling, M., Chand, D., Artaxo, P., Rizzo, L., Nishioka, G., Kolle, O., Fritsch, H., Silva Dias, M. A. F., Gatti, L. V., Cordova., A. M., Andreae, M. O.: Airborne measurements of trace gas and aerosol particle emissions from biomass burning in Amazonia, Atmos. Chem. Phys. Discuss., 5, 2791–2831, 2005, SRef-ID: 1680-7375/acpd/2005-5-2791.

Hobbs, P. V., Reid, J. S., Kotchenruther, R. A., Ferek, R. J., and Weiss, R.: Direct radiative forcing by smoke from biomass burning, Science, 275, 1776–1778, 1997.

Hobbs, P. V., Sinha, P., Yokelson, R. J., Christian, T. J., Blake, D. R., Gao, S., Kirchstetter, T. W., Novakov, T., and Pilewskie, P.: Evolution of gases and particles from a savanna fire in South Africa, J. Geophys. Res.-Atmos., 108(D13), 8485, doi:10.1029/2002JD002352, 2003.

Holben B. N., Eck, T. F., Slutsker, I., Tanre, D., Buis, J. P., Setzer, A., Vermote, E., Reagan, J. A., Kaufman, Y., Nakajima, T., Lavenu, F., Jankowiak, I., and Smirnov, A.: AERONET – A federated instrument network and data archive for aerosol characterization, Rem. Sens. Environ., 66, 1–16, 1998.

4394

Horvath, H. and Trier, A.: A study of the aerosol of Santiago de ChileFII: mass extinction coefficients, visibilities and Angstrom exponents, Atmos. Environ. 27A (3), 385–395, 1993.

Intergovernmental Panel on Climate Change (IPCC), Third Assessment Report, Climate Change 2001: The Scientific Basis, edited by: Houghton, J. T., Cambridge Univ. Press, New York, 2001.

Kirchstetter, T. W., Novakov, T., and Hobbs, P. V.,: Evidence that the spectral dependence of light absorption by aerosols is affected by organic carbon, J. Geophys. Res.-Atmos., 109(D21208), doi:10.1029/2004JD004999, 2004.

Kirkman, G. A., Gut, A., Ammann, C., Gatti, L. V., Cordova, A.M., Moura, M. A. L., Andreae, M. O., and Meixner, F. X.: Surface exchange of nitric oxide, nitrogen dioxide, and ozone at a cattle pasture in Rondônia, Brazil, J. Geophys. Res.-Atmos., 107, D20, 8083, doi:10.1029/2001JD000523, 2002.

Kotchenruther, R. A. and Hobbs, P. V.: Humidification factors of aerosols from biomass burning in Brazil, J. Geophys. Res.-Atmos., 103, 32 081–32 089, 1998.

Martins, J. V., Artaxo, P., Liousse, C., Reid, J. S., Hobbs, P. V., and Kaufman, Y. J.: Effects of black carbon content, particle size and mixing on light absorption by aerosol particles from biomass burning in Brazil, J. Geophys. Res.-Atmos., 103, 32 041–32 050, 1998.

Pickering, K. E., Thompson, A. M., Wang, Y. S., Tao, W. K., McNamara, D. P., Kirchhoff, V., Heikes, B. G., Sachse, G. W., Bradshaw, J. D., Gregory, G. L., and Blake, D. R.: Convective transport of biomass burning emissions over Brazil during TRACE A, J. Geophys. Res.-Atmos., 101, 23 993–24 012, 1996.

Procopio, A. S., Remer, L. A., Artaxo, P., Kaufman, Y. J., and Holben, B. N.: Modeled spectral optical properties for smoke aerosols in Amazonia, Geophys. Res. Lett., 30, 24, 2265–2270, doi:10.1029/2003GL018063, 2003.

Procópio, A. S., Artaxo, P., Kaufman, Y. J., Remer, L. A., Schafer, J. S., and Holben, B. N.: Multi-year analysis of Amazonian biomass burning smoke radiative forcing of climate, Geophysical Research Letters, 31, 3, L03108-L03112, doi:10.1029/2003GL018646, 2004.

Ramanathan, V., Crutzen, P. J., Kiehl, J. T., and Rosenfeld, D.: Aerosols, climate and the hydrological cycle, Science, 294, 2119–2124, 2001.

Reid, J. S. and Hobbs, P. V.: Physical and chemical properties of individual biomass fires in Brazil, J. Geophys. Res.-Atmos., 103, 32 013–32 030, 1998a.

Reid, J. S., Hobbs, P. V., Ferek, R. J., Blake, D. R., Martins, J. V., Dunlap, M. R., and Liousse, C.: Physical, chemical, and optical properties of regional hazes dominated by smoke in Brazil,

4395

J. Geophys. Res.-Atmos., 103, 32 059–32 080, 1998b.

Reid, J. S., Eck, T. F., Christopher, S. A., Koppmann, R., Dubovik, O., Eleuterio, D. P., Holben, B. N., Reid, E. A. and Zhang, J.: A review of biomass burning emissions, part III: intensive optical properties of biomass burning particles, Atmos. Chem. Phys. Discuss., 4, 5201–5260, 2004a,

SRef-ID: 1680-7375/acpd/2004-4-5201.

Reid, J. S., Koppmann, R., Eck, T. F. and Eleuterio, D. P.: A review of biomass burning emissions, part II: Intensive physical properties of biomass burning particles, Atmos. Chem. Phys. Discuss., 4, 5135–5200, 2004b,

SRef-ID: 1680-7375/acpd/2004-4-5135.

Rolph, G. D.: Real-time Environmental Applications and Display sYstem (READY) Website (http://www.arl.noaa.gov/ready/hysplit4.html). NOAA Air Resources Laboratory, Silver Spring, MD, 2003.

Rosenfeld, D.: Suppression of rain and snow by urban and industrial air pollution, Science, 287, 1793–1796, 2000.

Ross, J. L., Hobbs, P. V., and Holben, B.: Radiative characteristics of regional hazes dominated by smoke from biomass burning in Brazil: Closure tests and direct radiative forcing, J. Geophys. Res.-Atmos., 103, 31 925–31 941, 1998.

Satheesh, S. K. and Ramanathan, V.: Large differences in the tropical aerosol forcing at the top of the atmosphere and Earth's surface, Nature, 405, 60–63, 2000.

Schnaiter, M., Schmid, O., Petzold, A., Fritzsche, L., Klein, K.-F., Andreae, M. O., Helas, G., Thielmann, A., Grimmler, M., Möhler, O., Linke, C., and Schurath, U.: Measurement of wavelength-resolved light absorption by aerosols utilizing a UV-VIS extinction cell, Aerosol Sci. Technol., 39, 249–260, 2005.

Smirnov, A., Holben, B. N., Eck, T. F., Dubovik, O., and Slutsker, I.: Cloud screening and quality control algorithms for the AERONET data base, Remote Sens. Environ., 73, 337–349, 2000.

Terhune, R. W. and Anderson, J. E.: Spectrophone measurements of the absorption of visible light by aerosols in the atmosphere, Optics Letters, 1, 70–72, 1977.

Trebs, I., Meixner, F. X., Slanina, J., Oties, R. P., Jongejan, P., and Andreae, M. O.: Real-time measurements of ammonia, acidic trace gases and water-soluble inorganic aerosol species at a rural site in the Amazon Basin, Atmos. Chem. and Phy., 4, 967–987, 2004.

Trebs, I., Lara, L. B. L. S., Zeri, L. M. M., Gatti, L. V., Artaxo, P., Dlugi, R., Slanina, J., Andreae, M. O., and Meixner, F. X.: Dry and wet deposition of inorganic nitrogen compounds to a

4396

tropical pasture site (Rondônia, Brazil), Atmos. Chem. Phys. Discuss., 5, 3131–3189, 2005, SRef-ID: 1680-7375/acpd/2005-5-3131.

Weingartner, E., Saathoff, H., Schnaiter, M., Streit, N., Bitnar, B., and Baltensperger, U.: Absorption of light by soot particles: determination of the absorption coefficient by means of aethalometer, J. Aerosol Sci., 34, 1445–1463, 2003.

Table 1. Summary of the optical and physical properties of aerosols along with CO concentration at surface (S), boundary layer (BL) and free troposphere (FT) during the biomass burning season. The availability of measurements at S, BL and FT are shown by right ($\sqrt{}$) tick and the "x" shows the parameters with no observations.

Parameter with units	Symbols	Availability of measurements		
		S	BL	FT
Light scattering coefficient at 545, 550 nm (Mm^{-1})	σ_s	$\sqrt{}$	$\sqrt{}$	$\sqrt{}$
Light absorption coefficient at 532 nm (Mm^{-1})	σ_a	$\sqrt{}$	x	x
Condensation nuclei (cm^{-3}))	CN	$\sqrt{}$	$\sqrt{}$	$\sqrt{}$
Aerosol mass (g cm^{-3})	PM2.5	$\sqrt{}$	x	x
Aerosols optical thickness at 440, 670 nm	AOT	Column integrated		
Carbon monoxide (ppb)	CO	$\sqrt{}$	$\sqrt{}$	$\sqrt{}$
Mass scattering efficiency (σ_s normalized with PM2.5 $m^2 g^{-1}$)[†]	α_s	$\sqrt{}$	x	x
Mass absorption efficiency (σ_a normalized with PM2.5 $m^2 g^{-1}$)[†]	α_a	$\sqrt{}$	x	x
Single scattering albedo (using σ_s and σ_a)	ω_o	$\sqrt{}$	x	x
Excess ratio (dσ_s/dCN)	dσ_s/dCN	$\sqrt{}$	$\sqrt{}$	$\sqrt{}$
Excess ratio (dσ_s/dCO)	dσ_s/dCO	$\sqrt{}$	$\sqrt{}$	$\sqrt{}$
Excess Ratio (dσ_s/dPM2.5) or Mass scattering efficiency ($m^2 g^{-1}$)[††]	dσ_s/dPM2.5	$\sqrt{}$	x	x
Excess Ratio (dσ_a/dPM2.5) or Mass absorption efficiency ($m^2 g^{-1}$)[††]	dσ_a/dPM2.5	$\sqrt{}$	x	x

[†]) Based on average of all data, i. e., $\frac{1}{N} \sum_{i}^{N} \left(\frac{\sigma_s}{PM2.5} \right)_i$

[††]) based on correlations of σ_s and σ_a with PM2.5

Table 2. Correlations of light scattering coefficient (σ_s) with CO and CN from the airborne (boundary layer-BL and free troposphere-FT) and surface observations at FNS. The flights, shown by the respective numbers were conducted on the dates given in brackets in column 1. The correlation coefficients (r^2) of the slopes $d\sigma_s/dCN$ and $d\sigma_s/dCO$ are given in parenthesis. The factor "A" is the ratio of $d\sigma_s/dCN$ in the FT to BL [i.e., $[(d\sigma_s/dCN)_{FT}/(d\sigma_s/dCN)_{BL}]$. Similarly, the factor "B" is the ratio of $d\sigma_s/dCO$ in the FT to BL [i.e., $[(d\sigma_s/dCO)_{FT}/(d\sigma_s/dCO)_{BL}]$. The factor "C" is the ratio of ($V_n=V/N$) in the FT (2500 m) to that in the BL (500 m) [i.e., $[(V_n)_{FT}/(V_n)_{BL}]$ with total volume (V) and number of aerosols (N) in the size range 42–346 nm (aerodynamic diameter D_p). The wavelengths of σ_s from the airborne and surface platforms were 550 and 545 nm, respectively.

	Flight No (Date)	$(d\sigma_s/dCN)_{BL}$ ($Mm^{-1}\,cm^{-3}$)	$(d\sigma_s/dCN)_{FT}$ ($Mm^{-1}\,cm^{-3}$)	$(d\sigma_s/dCO)_{BL}$	A	B	C
Airborne	4 [28 September]	0.011 (0.14)	0.12 (0.79)	0.36 (0.55)	10.9	2.8	1.6
	6 [30 September]	0.015 (0.64)	0.037 (0.76)	0.38 (0.67)*	2.4	–	1.3
	7 [30 September]	0.018 (0.76)	0.026 (0.50)	0.38(0.67)*	1.4	–	1.3
	08 [1 October]	0.019 (0.57)	0.033 (0.55)	0.38(0.67)*	1.7	–	1.3
	24 [15 October]	0.019 (0.57)	0.076 (0.73)	0.40 (0.60)	4.0	3.8	1.6
Surface	16 Sep. – 8 Oct.	0.03 (0.30)	–	0.42 (0.88)	–	–	–

* The average slope $(d\sigma_s/dCO)_{BL}$ of the flights 5, 7, 8 (see Fig. 4).

4399

Table 3. Average Ångström exponent calculated from the airborne (nephelometer, $\overset{0}{a}_s$) and integrated (sunphotometer, $\overset{0}{a}_e$) observations. The wavelengths λ_1 and λ_2 used for computing the Ångström exponent from the nephelometer and the sunphotometer are 450–700 nm and 440–670 nm. In addition to the average $\overset{0}{a}_e$ during the airborne observation days, an average Ångström exponent is also calculated for the entire burning period. SD represents the standard deviation from the number of observations shown by the counts. Each count from airborne observations is 1 s whereas for the sunphotometer it is about 15 min.

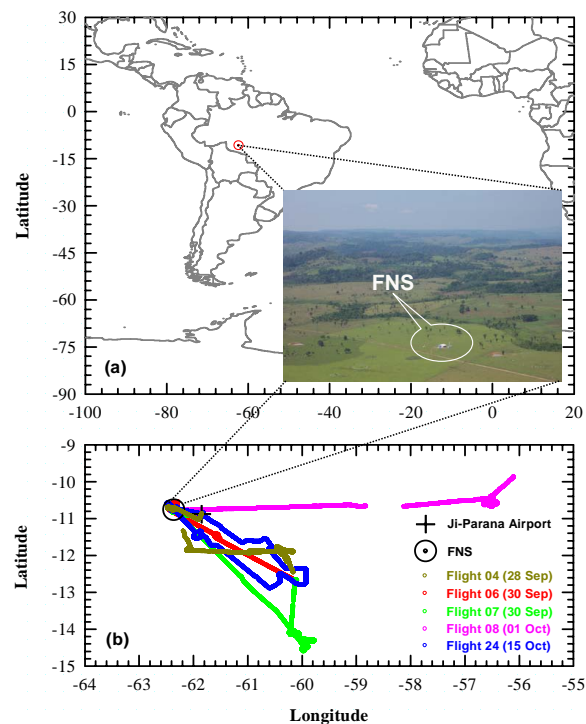| Observations	Flight No (Date)	Ångström Exponent, $\overset{0}{a}_s$ (450–700 nm) Airborne nephelometer			Ångström Exponent $\overset{0}{a}_e$ (440–670 nm) Sunphotometer		
		Avg.	SD	Counts	Avg.	SD	Counts
	– (21 September)	–	–	–	1.74	0.05	8
	– (25 September)	–	–	–	2.01	0.04	11
	– (5 October)	–	–	–	1.85	0.02	10
	4 (28 September)	1.90	0.33	10 106	1.70	0.05	11
	6 (30 September)	1.98	0.41	8103	1.57	0.04	7
	7 (30 September)	2.06	0.35	11 149	1.57	0.04	7
	8 (1 October)	2.11	0.31	5269	1.40	0.13	13
	24 (15 October)	1.98	0.19	13 166	1.53	0.06	3
Burning period	(16–27 September)	–	–	–	1.77	0.17	122

4400

Fig. 1. (a) Overview map showing the geographical location of the surface site FNS. The picture is an aerial view of the site. **(b)** Flight tracks for flights 4, 6, 7, 8, and 24. The positions of FNS and the nearby Ji-Paraná airport are shown by the circle and cross symbols, respectively.
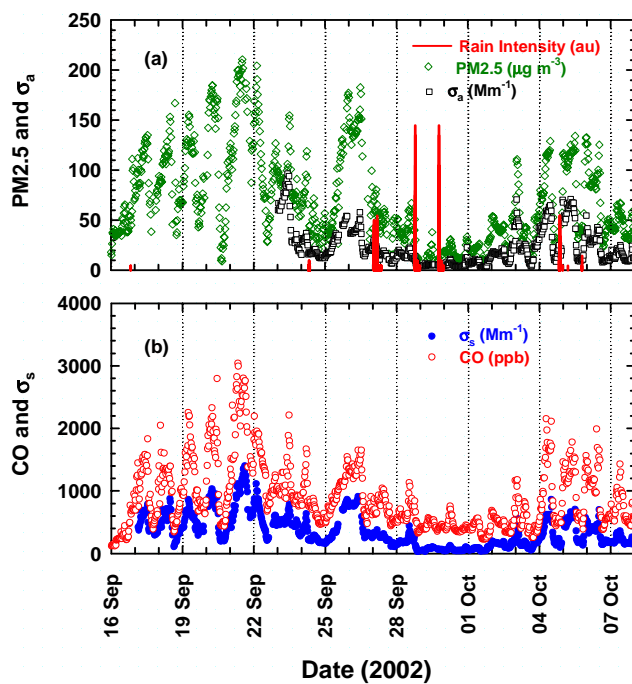
4401

Fig. 2. Temporal variation of PM2.5 (diamonds), light absorption coefficient (σ_s, squares), light scattering coefficient (σ_s, solid circles) and CO mixing ratio (open circles) at 30-min intervals in the biomass burning season at the surface station (FNS). The rainfall (arbitrary units) is shown by the vertical bars.
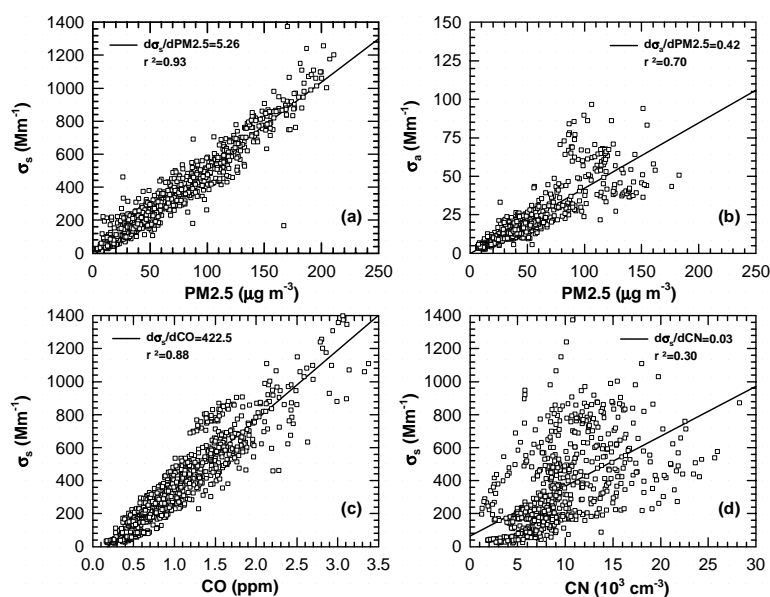
4402

Fig. 3. Scatter plots and regression lines for 30-min averaged data of **(a)** light scattering coefficient (σ_s) versus aerosol mass concentration (PM2.5) at the ground station (FNS) during the biomass burning season. Similarly, **(b)** the light absorption coefficient (σ_a) versus PM2.5, **(c)** σ_s versus CO, and **(d)** σ_s versus aerosol number concentration (CN). The slopes are least-square-fitted lines. The corresponding correlation coefficients (r^2) of these parameters are shown on the respective plates.
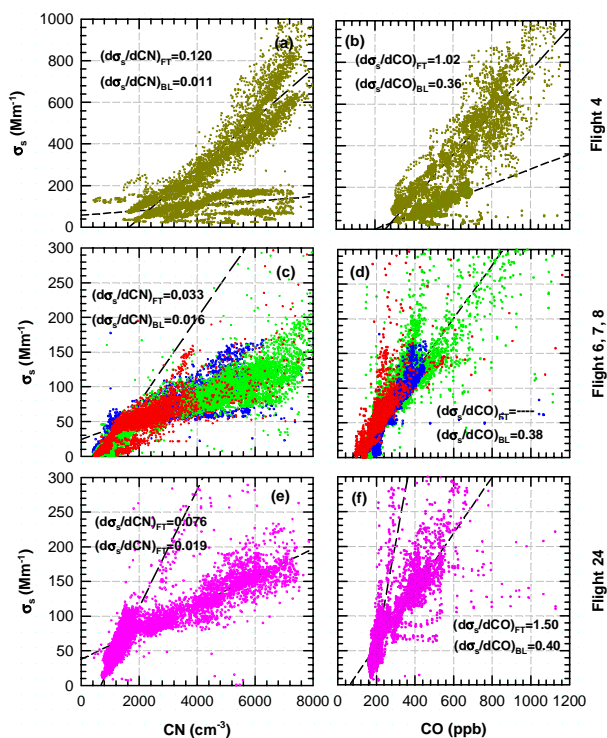
4403

Fig. 4. Scatter plots and regression lines of the light scattering coefficient (σ_s) from the airborne observations at 550 nm against aerosol number concentration (CN) and CO for flight 4 **(a, b)**; flights 6, 7, 8 **(c, d)**; and flight 24 **(e, f)**. Data for different flights are shown by different colors. The slopes in the BL and FT are shown by the dashed and long dashed lines.
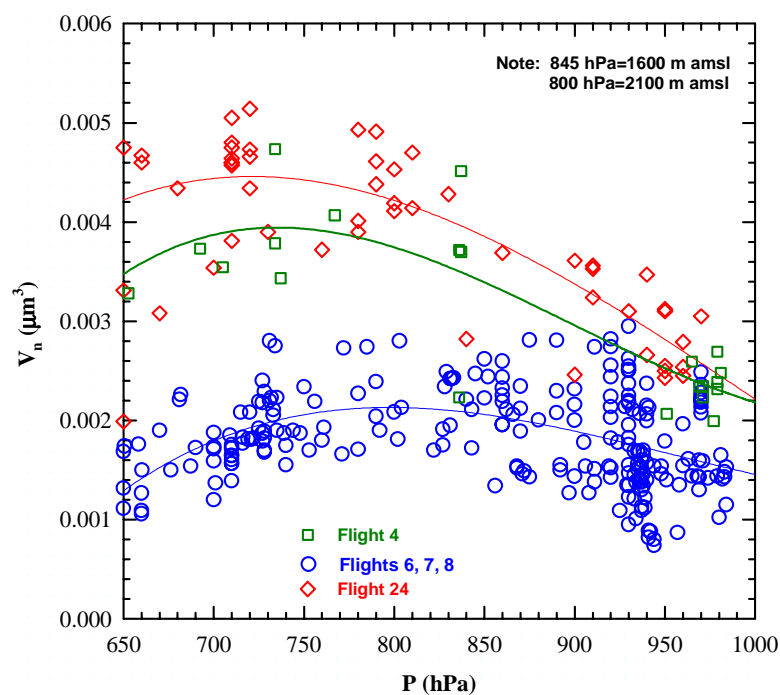
Fig. 5. Vertical variation in number-normalized total volume of aerosol (V_n) in the size range 42–346 nm (aerodynamic diameter, D_p) during the flights 4, 6, 7, 8 and 24. The curves are fits based on the least squared method.
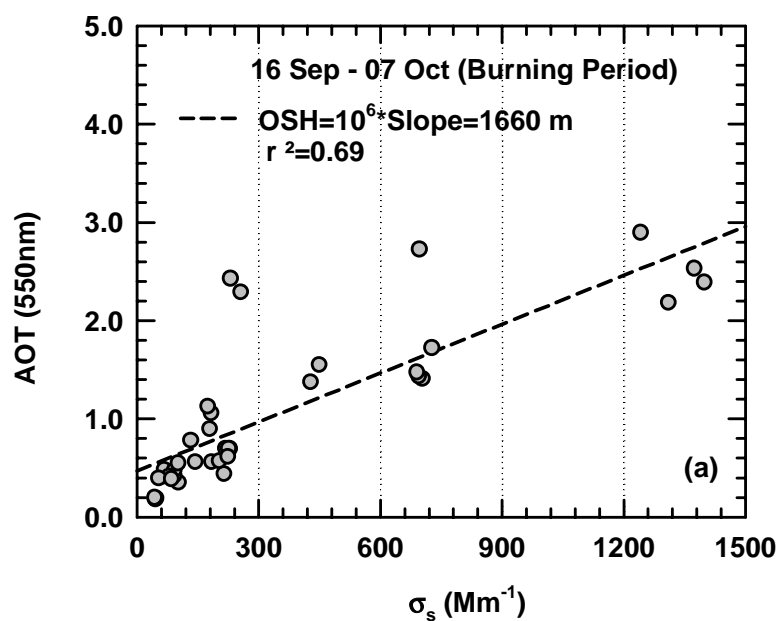
Fig. 6. Scatter plot of light scattering coefficient (σ_s) with aerosol optical thickness (AOT) (both σ_s and AOT at 550 nm) during the biomass burning season (16 September–7 October). The AOT data are taken between 11:00 to 14:00 LT. The OSH and the correlation coefficient (r^2) also given in the figure.